Lattice performance during initial steps of the Smart-Cut™ process in semiconducting diamond: A STEM study

J.C. Piñero, J. de Vecchy, D. Fernández, G. Alba, J. Widiez, L. Di Cioccio, F. Lloret, D. Araujo, Julien Pernot

Lattice performance during initial steps of the Smart-Cut™ process in semiconducting diamond: a STEM study

J.C. Piñero*[,a], J. de Vecchy[b], D. Fernández[c], G. Alba[c], J. Widiez[b], L. Di Cioccio[b], F. Lloret[c], D. Araujo[d], J. Pernot[e]

[a]*Departamento de Didáctica, área de Matemáticas. Universidad de Cádiz, 11510, Spain*
[b]*Univ. Grenoble Alpes, CEA, LETI, 38000 Grenoble, France*
[c]*Departamento de Física Aplicada. Universidad de Cádiz, 11510, Spain*
[d]*Departamento de Ciencias de los Materiales, IM y QI. Universidad de Cádiz, 11510, Spain*
[e]*Institut Néel, CNRS-UJF, av. des Martyrs, 38042 Grenoble, France*

Keywords:
Diamond
Schottky
Oxygen-terminated
TEM
Power devices

A B S T R A C T

An alternative route for the development of diamond-based technologies is the Smart-Cut process. Such a process could make possible the combination of diamond and silicon technologies, as well as building alternative structures or manufacturing large diamond wafers. However, crystalline quality and implantation-related damages may alter the electronic properties of the diamond wafer. In fact, this is a critical bottleneck that needs to be analysed in order to develop a reliable diamond/Smart-Cut based technology. In this contribution, we present STEM-based experiments used to evaluate various key parameters such as the sharpness of the transition regions, the behaviour of the implanted region and diamond lattice performance in Smart-Cut processes. Indeed, an outstanding sp^2/sp^3 relation close to ideality (it is, that of undamaged diamond) is evidenced in the diamond-transfer region.

1. Introduction

The Smart-Cut technology (a registered trademark of SOITEC) enables the transfer of very fine and crystalline material layer onto a mechanical support [1]. The usual process consists of 3 main technological steps the hydrogen implantation inside a donor wafer, a bonding to a receiving wafer and a fracture treatment that enables the material splitting parallel to the donor surface (see Fig.1). So far, this method has been successfully developed to transfer a large number of materials such as Si [2], Ge [3], SiGe [4], SiC [5], GaN [6], and is here being considered to transfer semiconducting diamond wafers. A successful application of this procedure is possible by controlling the ion implantation depth as well as the sharpness of the implanted/not implanted transition. Indeed, these are key aspects to be studied when considering the application of this technology for transferring semiconducting diamond sheets.

However, diamond sheet transfer based on ion-beam operations might not be exempt of difficulties. The major bottleneck for ion-beam operations in diamond is related with the graphitization or amorphization of the diamond lattice. This amorphization might be an undesired byproduct of Focused Ion Beam sample preparation [7], ion-beam doping [8], or the proposed sheet transfer procedure. Indeed, ion implantation in diamond crystals may induce damage in the lattice depending on the voltage, dose, incident ions, angle of incidence, annealing temperature, annealing time and other parameters. Eventually, such damages might be over the graphitization limit [9], even when light incident ions are used [10, 11].

So, the implanted ions have to be chosen to reduce potential damages in the transfer layer. In this regard “light” ions are expected to be less destructive. Analyzing potential candidates, O species induce much more damages in implanted semiconducting diamond (because of its large size). In the literature, oxygen implantation has been used to create a graphitized layer but the appearance of bubbles after annealing (which should ease exfoliation) has not been

* *Corresponding author.* Tel.: +34 660 584895; fax: +0-000-000-0000.
E-mail address: josecarlos.pinero@uca.es

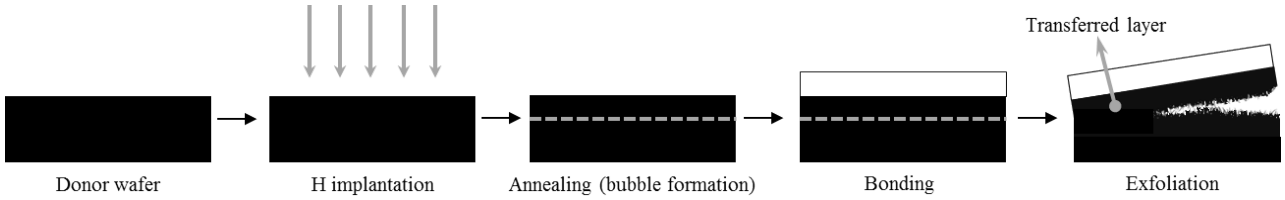

Fig.1: Technological steps conventionally used in a Smart-Cut process. The main steps consist of hydrogen implantation inside a donor wafer, an annealing to induce bubble formation, a bonding to a receiving wafer and a fracture treatment that enables the material splitting parallel to the donor surface.

mentioned [12, 13]. However, previous manuscripts reports that various kinds of implanted species or implantation induced defects can act as efficient traps for H and then promote platelets and microcracks formation [14]. Additionally, some authors have been able to create conductive hydrogen-implanted diamond layers by using an appropriate annealing process [15, 16]. Furthermore, the conditions presented by some authors [17] allow to identify possible blistering conditions using two H^+ implantation/annealing combinations. So, our interest in this research is to find a process using H^+ incident ions at keV acceleration which creates optimum blistering conditions (it is, conditions needed for the bubble formation mentioned in Fig.1).

The transfer of semiconducting diamond using the Smart-Cut technology is a promising way to manufacture diamond wafers, due to the significant limitations in single crystal diamond (SCD) substrate size [18] which hampers the development of large (>1 in.) high-quality SCD wafers. Additional applications for this technology might be related with the possibility of building vertical diamond-based devices; opening the gate to a brand new world of possible architectures. On the other hand transferring large, thin diamond layers should ease the combination of Si or SiC technologies with the emergent diamond technology. However, to our knowledge, blistering conditions in diamond have not been identified yet.

A damaged diamond lattice would affect the electric performance of the related layer [19]. This could be a bottleneck for the technological application of diamond sheet transfer using the Smart-Cut process. So, semiconducting diamond presents specific challenges for a Smart-Cut process. Here, we propose two steps combining implantation/annealing. The scope of the first step of the diamond Smart-Cut procedure is to implant H^+ ions inside a crystalline structure avoiding a maximum of defects in order to weaken the material in a parallel plain of the surface. The "bubbles formation" step should appear after the second implantation/anneal step. However, tracking the behaviour of the lattice during the different steps of a Smart-Cut process in semiconducting diamond becomes necessary (as the transferred layer might be damaged during the first implantation).

The previously described challenges (potential lattice damages, control of the ion implantation depth and sharpness of the transition) are here evaluated. In this regard, this manuscript studies the first set of combined implantation/annealing step of the proposed two-step procedure. The scope of this study is to evaluate the crystallinity of the diamond sheet-transfer lattice after the first set of implantation/annealing. To do so, structural characterization of H^+ ion-implanted diamond is carried out by using a variety of Scanning Transmission Electron Microscopy (STEM)-related techniques.

Table 1 Implantation parameters (H^+ incident ions) and annealing conditions used in the different regions of the sample.

	Dose (cm^{-2})	E_i (KeV)	Annealing	
			Temperature (ºC)	Time
LD	$5x10^{16}$	60	1000	1h
MD	$1.4x10^{17}$	60	1000	1h
HD	$3x10^{17}$	60	1000	1h

2. Experimental procedure

H^+ ions were implanted on a commercial diamond substrate of the LakeDiamond society. This Ib high pressure high temperature (HPHT) substrate has a rugosity below 3nm, being {100} oriented and with $3x3x0.3mm^3$ dimensions. The sample was in-situ cleaned by hydrogen plasma. Accelerating voltages of hydrogen incident H^+ ions was fixed at 60keV, while the ion dose was shifted to design three implantation regions with low/medium/high ion doses, labelled as LD, MD and HD regions. Details of the implantation doses are summarized in Table 1, such parameters were chosen to fit to that of literature [20]. Finally, the sample was annealed at 1000ºC during one hour (under 10^{-8}mbar pressure) to induce crystalline reconstruction.

The final structure of the sample is presented in Figure 2, where three different implantation regions are evidenced and highlighted with white, dashed lines. White arrows in Fig.2 indicate the position where FIB lamellas were prepared. Concerning the TEM lamella preparation, samples were nano-machined with the Ga^+ ion beam of a Quanta 200 3D dual-beam Focused Ion Beam (FIB) system. Electron-transparent specimens (≈100nm thick) were characterized by using a FEI-TITAN THEMIS electron microscope.

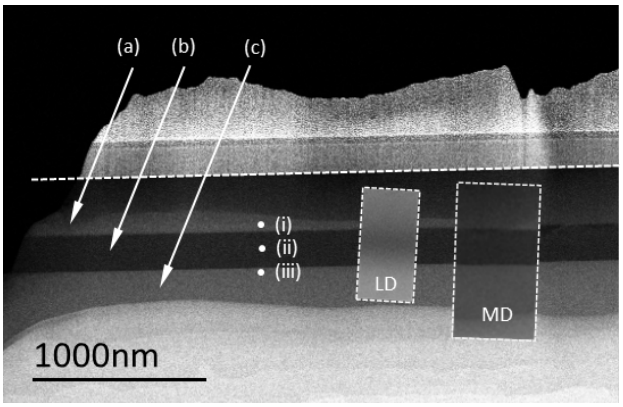

Fig.4: HAADF micrography of a FIB-lamella prepared in the HD region. The H^+-implanted layer (b) is revealed as a dark contrast right between the diamond sheet (a) and the diamond bulk (c). Inset shows ADF and HAADF images obtained in MD and LD regions

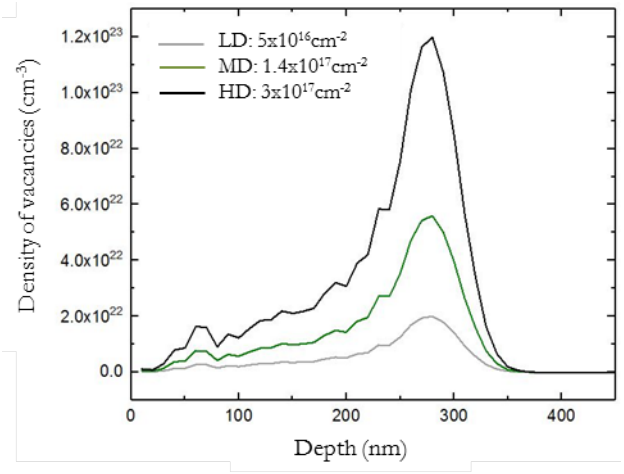

Fig.3: Density of vacancies vs implantation depth, as simulated by SRIM for the implantation doses presented in Table 1.

3. Results and discussion

As previously highlighted, ion implantation in diamond crystals may induce damage in the lattice. Moreover, implantation depth and sharpness of the implanted/not implanted transition are key parameters to be considered in this study. Indeed, H^+ ions should pass through the top surface, having a Gaussian-like repartition on the semiconductor material (as presented Fig. 3, where a SRIM simulation [21, 22] of the ion implantation is presented). Here, a complete characterization of the sharpness of the transition and the crystalline quality are carried out by analyzing different samples with a variety of STEM-related techniques.

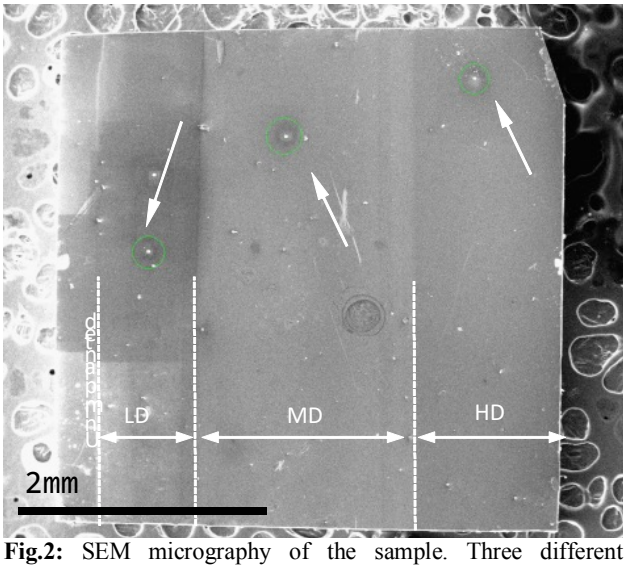

Fig.2: SEM micrography of the sample. Three different implantation regions are revealed. White arrows and green circles indicate the position where FIB specimens were extracted.

3.1. STEM-HAADF

Figure 4 shows a High Angle Annular Dark Field (HAADF) micrography obtained on the FIB lamella prepared in the HD region. White dashed line in Fig.4 is used to highlight the top diamond surface. Above that line, a protective Pt layer (deposited during FIB operation) is revealed.

HAADF contrasts are related with the Z-number of the material and with the specimen thickness. This allows identifying three different layers right below the white dashed line:

(a) This layer has not been implanted, but has been overpassed by H^+ ions. However, H atoms that are implanted in deeper layers might induce lattice damages. This is also the diamond sheet to be transferred, so the structural and electrical qualities of this layer would define the suitability of the Smart Cut procedure.

(b) This layer corresponds with the H-implanted region, located at 250nm depth.

(c) Finally, layer (c) corresponds with the diamond bulk, not implanted nor damaged.

.

HAADF micrographies obtained in FIB lamellas prepared in the MD and LD regions are shown as insets in Fig.4. Inset corresponding with the MD region reveals a HAADF contrast similar to that obtained in the HD region. However, a minor change in the feature of the HAADF contrast is evidenced in the LD region, where Z-contrast among the different layers is negligible (it is, there is almost no Z change between the different layers).

3.2. HR-STEM

High Resolution (HR)-STEM images were obtained in the (i), (ii) and (iii) positions highlighted in Fig.4. Each position corresponds with the analysis of the a-b-c layers described

in section 3.1

Figure 5a and 5e shows HR-STEM micrographies obtained in positions (i) and (iii) (corresponding with layers (a) and (c) of the lamella obtained in the HD region, respectively). Crystalline behaviour is evidenced in both layers. Crystalline behaviour in layer (c) was expected because no ions were implanted in this region. However, crystalline behaviour of layer (a) has to be highlighted because this layer has been overpassed by H^+ ions and one can expect some crystalline damage remaining. Furthermore, Selected Area Diffraction Patterns (SAED) obtained in positions (i) and (iii) (Fig.5b and 5f) confirm the crystalline behaviour: diffraction spots are clearly evidenced with no amorphous behaviour remaining. Finally, HR-STEM micrographies show Dumbbell structure of the diamond crystal, where two-spot structures (corresponding with two kinds of atomic columns composing the crystal) are detected. White and black contrasts correspond to carbon atomic columns and vacuum tunnels respectively. Inset in Fig.5e shows schematic plot of the diamond lattice in the selected crystalline orientation, to ease the understanding of the HR-STEM feature.

On the other hand, HR-STEM data were obtained in position (ii), corresponding with layer (b). Such layer has been H-implanted and annealed. No crystalline behaviour is evidenced by HR-STEM (see Fig.5c) nor SAED (see Fig.5d) in the HD region. Fig.5c compares the HR-STEM data obtained in the LD and HD regions. It can be observed that LD-related data reveals crystalline behaviour. HR-STEM data were also collected on MD region, obtaining identical micrographies to that obtained in the HD region. As a result, one can conclude that the implanted layer (b) has an amorphous structure in the HD and MD regions, while layer (a) is not damaged by the incident H^+ ions –its crystalline quality is comparable to that of the bulk-. However HR-STEM and SAED data obtained in FIB lamella prepared in the LD region shows crystallinity, which is coherent with HAADF experiments. No differences in the crystalline quality of the (a) and (c) layers have been detected.

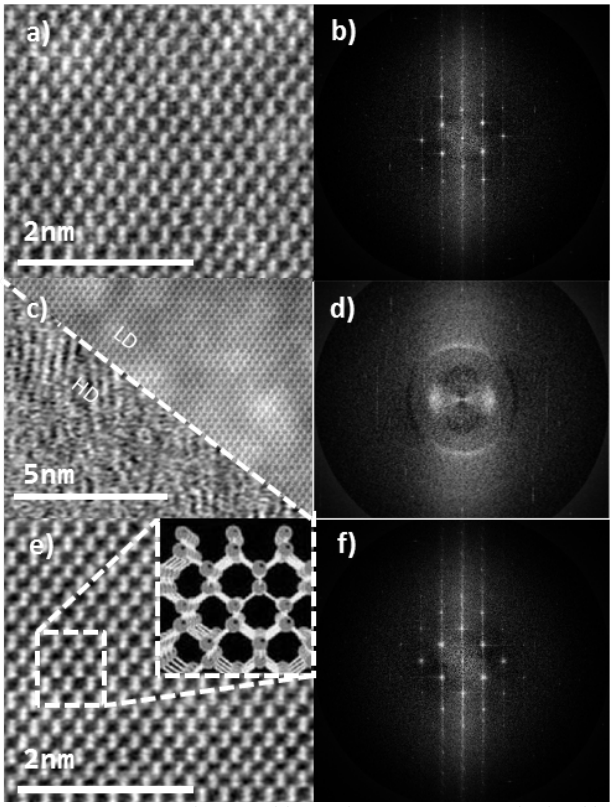

Fig.5: HR-STEM micrographies and SAED patterns obtained in positions (i), (ii) and (iii) as presented in Fig.4. Crystalline behavior is observed in positions (i) and (iii) (corresponding with Fig.5a and Fig.5e), while amorphous behavior is evidenced in position (ii) (corresponding with Fig.5c).

3.3. STEM-EDS

Energy Dispersive X-ray Spectroscopy (EDS) maps were obtained in FIB lamella prepared in the HD region. EDS is an analytical technique used for the elemental analysis or chemical characterization of a sample, consisting on the interaction of an electron source that stimulates the emission of characteristic X-rays of the specimen. As the energies of the X-rays are characteristic of the difference in energy between the two shells and of the atomic structure of the emitting element, EDS allows the elemental composition of the specimen to be measured. However, EDS provides "arbitrary units" intensity counts, so that we can only evaluate the differences arising from different amount of material at different positions of the sample. So, contrasts in EDS maps are related with differences in the amount of material, but cannot be exactly quantified. However, EDS provides enough information to estimate the relative C and O content from the EDS intensity.

Figure 6 shows EDS maps corresponding to the C and O peaks. A 200nm thick layer is evidenced in both maps, corresponding with the H-implanted layer. In the particular case of the C map, a decrease of the C content in the mentioned layer is evidenced and the relative intensity allows estimating a variation of 5% in the carbon content. Furthermore, this layer corresponds with layer (b) presented in Fig.4 (which shows an amorphous behaviour in the HR-STEM analysis). One can easily conclude that C atoms have been displaced from their original positions of the lattice, creating an amorphous layer. Stopping the incident hydrogen ions produces damages in the diamond lattice, experimenting amorphization. The resulting amorphous material has lower atomic density than the crystalline diamond.

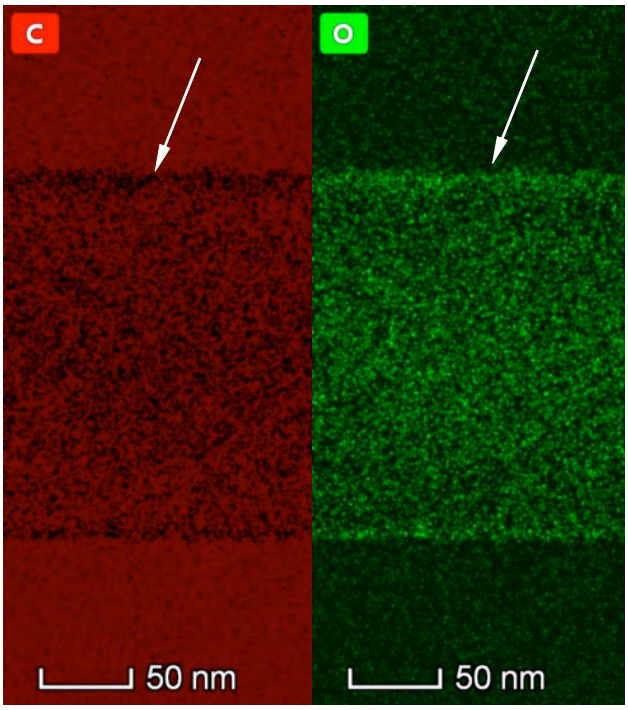

Fig.6: Carbon and oxygen EDS maps obtained in the FIB lamella prepared in the HD region. Layers a-b-c, presented in Fig.4, are revealed. A decrease of the C content is evidenced in layer (b). White arrows indicates the interface of the (a) and (b) layers, highlighting a strong decrease of the C content (while an increase of the O content is revealed).

On the other hand, a strong decrease of the C content is revealed in both interfaces (see white arrow in Fig.6). This feature corresponds with a higher O concentration. We think that O atoms might be captured in the sample surface during the lamella transfer from FIB to STEM microscopes: Ion implantation may increase the reactivity of the surface, so the presence of oxygen is basically an artefact induced by the FIB sample preparation (but is not related to the Smart-Cut process). A higher O concentration, accompanied by a lower C density in the interfaces might ease the exfoliation in a future technological step.
EDS data obtained in MD region shows identical behaviour.

3.4. STEM-EELS

Experimental EELS spectra were recorded in line-scan configuration, perpendicularly to the interface and passing through a-b-c layers in LD, MD and HD samples. The scope of this procedure is to measure the absorption of π* states, arising from sp^2 hybridation of carbon atoms. On the other hand, σ* states can also be detected by EELS. The related EELS intensities (labelled as I_{π^*} and I_{σ^*} respectively) are then used to establish the sp^2/sp^3 ratio. Such an intensity ratio is a measurement of the sp^2/sp^3 hybridation ratio and, therefore, a measurement of the amorphization ratio [23].
Figure 7 shows EELS spectra acquired in FIB lamella prepared in the HD region, EELS data corresponding to a-b-c layers and a-b transition are presented. Black-dashed lines are used to highlight the position of π* and σ* transition related peaks. A different behaviour of such peaks can be observed, with a meaningful arising of the π* peak in the (b) layer. This feature can be related with the amorphization of the (b) layer. For comparison, (a) and (c) layers show pure diamond EELS spectra. EELS data (presented in Fig.7) show the π* related peak, at 285eV. The appearance of the π* related peak can be used to track the sharpness of the (a)-(b) and (b)-(c) transitions and to quantify the sp^2/sp^3 ratio.
To track the sp^2/sp^3 ratio, a modification of the Cuomo expression [23] was proposed [9], so that the sp^2/sp^3 ratio becomes zero on pure diamond region (correcting a 15%

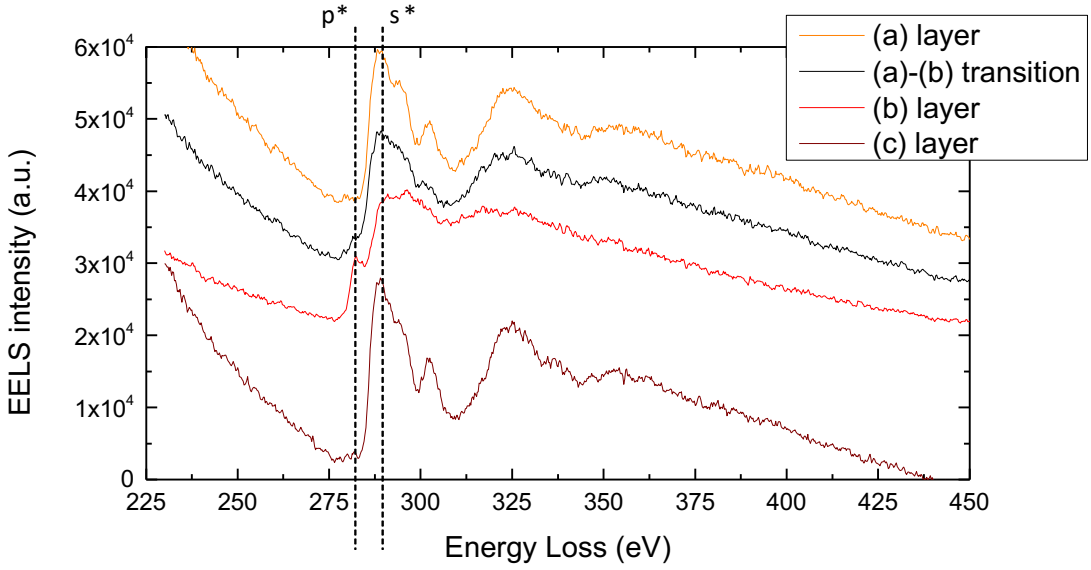

Fig.7: EELS spectra acquired at different locations of the a-b-c layer structure (HD sample). π* and σ* peak position are highlighted.

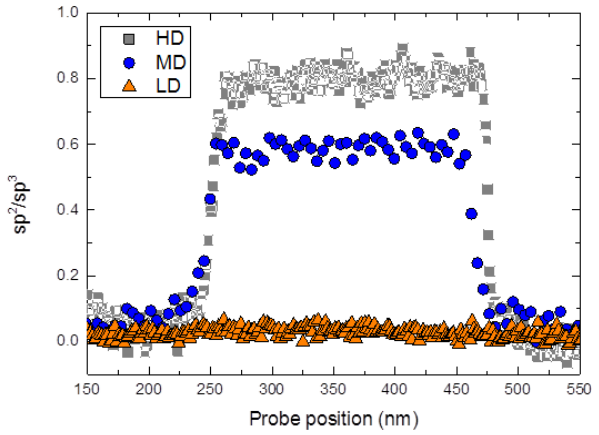

Fig.8: sp^2/sp^3 proportion vs EELS probe position (depth) for HD, MD and LD regions. Note that the implanted layer for all doses shows amorphous behavior while non-implanted layers show identical sp^2/sp^3 proportion.

error that is introduced when using the Cuomo expression). So the sp^2/sp^3 ratio can be calculated from:

$$\frac{I_{\pi^*} - 0.067}{I_{\sigma^*}} = \frac{3x}{4 - x} \qquad (1)$$

where x is the sp^2/sp^3 proportion, I_{π^*} the EELS integrated intensity using an energy window between 284 and 289 eV and I_{σ^*} the EELS integrated intensity with an energy window between 290 and 305 eV. With this procedure, the sp^2/sp^3 ratio vs EELS probe position is extracted.

Figure 8 shows sp^2/sp^3 proportion (x in Eq.1) versus EELS probe position (depth), as calculated from EELS data obtained in LD, MD and HD regions. Figure 8 evidences that sp^2/sp^3 proportion in MD and HD regions is not homogeneous, showing values close to zero in non-implanted layers (it is pure, undamaged diamond). On the other hand, a sp^2/sp^3 proportion close to unity is evidenced in the HD region right in the layer which corresponds to the H implantation (it is, amorphous C layer). Indeed, sp^2/sp^3 proportion calculated in HD and MD regions evidences amorphization of the diamond lattice. However, sp^2/sp^3 proportion calculated in the LD region shows no variations: no layer structure is evidenced. This result is coherent with that obtained by HAADF and HR-STEM.

Finally, sp^2/sp^3 depth profile is also useful to determine the sharpness of the transition, which is shown to be around 20nm. Note that accuracy on the determination of this sharpness transition is limited by sample thickness, drift in STEM, alignment of the TEM beam and other experimental issues (so this transition might be even sharper than 20 nm).

4. Conclusions

In this study, a variety of STEM-based techniques (EDS, EELS, HR-STEM…) have been used to evaluate the lattice performance during the first steps of the diamond Smart-Cut process. On this manuscript, it has been evidenced that the carbon content differs from one layer to another. Indeed, the amount of carbon in layer (a) –it is, the layer to be transferred- remains constant and is not altered by the pass of the ions through this layer to layer (b). Additionally, layer (b) –it is, the maximum implanted layer- register a minor amount of carbon when compared to layer (a), indicating a minor amorphization of the layer. On the other hand, EDS data shows that during sample manipulation (it is, when transferring the sample from FIB to STEM), sample is oxidized.

EELS and HR-STEM experiments are coincident and makes evident that the annealing process makes the first diamond layer –labelled as (a)- crystalline, while amorphization remains in layer (b), which corresponds to the region of maximum implantation. This is expected because EDS experiment shows that (b) layer has at least 5% less C content than the other layers. The features described for layer (a) are identical in HD, MD and LD regions.

Finally, a transition zone of around 20nm is revealed in (a)-to-(b) and in (b)-to-(c) interfaces. This feature is identical in HD and MD regions.

These results are in good agreement with the original scope of the Smart-Cut procedure: to implant H^+ ions inside a crystalline structure while avoiding a maximum of defects in the non-implanted layers, in order to weaken the material in a parallel plane of the surface.

Implications of this study demonstrate possibility of using Smart-Cut process for producing diamond layers with reliable structural properties. Indeed, this study demonstrate that (when using the implantations conditions here stated) a final annealing of 1000ºC results in a non-damaged diamond layer, with enough quality for being used in Smart-Cut sheet transfer. This found is to be well considered, because most of the available literature has concluded that a 1300ºC annealing is needed [24, 25], while few reports have been made on a successful annealing below that temperature [16]. This study concludes that diamond lattice is preserved after H^+ implantation, so structural properties remains useful for electrical purposes, opening the gate for Smart-Cut process in semiconducting diamond. Finally, another interesting characterization could be a TEM study with in situ annealing, this time placing the plates on a heating device transparent to electrons. This would enable tracking the diamond's behaviour during the first annealing and then the formation of gas bubbles during the second annealing of the process.

Acknowledgements

We thank the Ministerio de Economía y Competitividad (MINECO) of the Spanish Government for funding under Grants No. TEC2017-86347-C2-1-R (DiamMOS project) and No. ESP2017 - 91820 - EXP (Diam-Air, EXPLORA project) from FEDER funds. We thank to EU Frame- work Programme for research ¬ Innovation – H2020 for funding under Grant No. SEP-210184415 (GreenDiamond project) of H2020-LCE-2014-1.640947 program.

REFERENCES

1. Bruel, M., *Silicon on insulator material technology.* Electronics Letters, 1995. **31**(14).
2. M. Bruel, B.A., A.J. Auberton-Hervé, *Smart-Cut: A new Silicon On Insulator material technology based on hydrogen implantation and wafer bonding.* Jpn. J. Appl. Phys., 1997. **36**(1-3B): p. 1636-1641.
3. E. Augendre, L.S., L. Benaissa et al., *Challenges and Progress in Germanium-on-Insulator Materials and Device Development towards ULSI Integration.* ECS Transactions, 2009. **25**(7): p. 351-362.
4. J. Widiez, F.M., J-M. Hartmann et al., *SOI-type Bonded Structures for Advanced Technology Nodes.* ECS Transactions, 2014. **64**(5): p. 35-48.
5. L. Di Cioccio, Y.L.T., F. Letertre, C. Jaussaud and M. Bruel, *Silicon carbide on insulator formation using the Smart Cut process.* Electronics Letters, 1996. **32**(12): p. 1144-1145.
6. A. Tauzin, T.A., M. Rabarot, J. Dechamp, M. Zussy, H. Moriceau, J.F. Michaud, A.M. Charvet, L. Di Cioccio, F. Fournel, J. Garrione, B. Faure, F. Letertre and N. Kernevez, *Transfers of 2-inch GaN films onto sapphire substrates using Smart Cut technology.* Electronics Letters, 2005. **41**(11): p. 668.

   McKenzie, W.R., et al., *Focused Ion beam implantation of diamond.* Diamond and Related Materials, 2011. **20**(8): p. 1125-1128.
8. Fontaine, F., et al., *reality of doping by boron implantation of cvd polycrystalline diamond from a comparison of raman and electrical measurements.* Diamond and Related Materials, 1994. **3**(4-6): p. 623-627.
9. Piñero, J.C., et al., *Impact of Thermal Treatments in Crystalline Reconstruction and Electrical Properties of Diamond Ohmic Contacts Created by Boron Ion Implantation.* Physica Status Solidi (a), 2017. **214**(11): p. 1700230.
10. A.A. Gippius, R.A.K., V. A. Dravin, A.V. Khomich, *Defect-induced graphitisation in diamond implanted with light ions.* Physica B : Condensed Matter, 2001. **308**: p. 573-576.
11. A. A. Gippius, R.A.K., V. A. Dravin, A. V. Khomich, *Diamond - graphite transformation induced by light ions implantation.* Diamond and Related Materials, 2003. **12**: p. 538-541.
12. T. N. Tran Thi, B.F., D. Eon, E. Gheeraert, J. Härtwig, T. Lafford, A. Perrat-Mabilon, C. Peaucelle, P. Olivero, and E. Bustarret, *Ultra-smooth single crystal diamond surfaces resulting from implantation and lift-off processes.* Physica Status Solidi (a), 2011. **208**(9): p. 2057-2061.
13. N.R. Parikh, J.D.H., E. McGucken, M.L. Swanson, C.W. White, R.A. Rudder, D.P. Malta, J.B. Posthill and R.J. Markunas, *Single-crystal diamond plate liftoff achieved by ion implantation and subsequent annealing.* Appl Phys Lett, 1992. **61**.
14. Terreault, B., *Hydrogen blistering of silicon: Progress in fundamental understanding.* Physica Status Solidi (a), 2007. **204**(7): p. 2129–2184.
15. V.P. Popov, L.N.S., O.V. Naumova, D.V. Nikolaev, I.N. Kupriyanov, Yu.N. Palyanov, *Conductive layers in diamond formed by hydrogen ion implantation and annealing.* Nuclear Instruments and Methods in Physics Research Section B : Beam Interactions with Materials and Atoms, 2012. **288**(Ion Beam Synthesis and Modfication of Nanostructured Materials and Surfaces): p. 100-107.
16. V.P. Popov, L.N.S., O.V. Naumova, D.V. Nikolaev, Y.N. Palyvanov and I.N. Kupriyanov, *Diamond - graphite heterostructures formed by nitrogen and hydrogen implantation and annealing.* Advanced Materials Research, 2011. **276**(8).
17. Jaekwon Suk, H.K., Weon Cheol Lim, Jiwon Yune, Sung Moon, John A. Eliades, Joonkon Kim, Jaeyong Lee, Jonghan Song, *Fabrication of thin diamond membranes by using hot implantation and ion-cut methods.* Appl Phys Lett, 2017. **110**.
18. Meiyong Liao, B.S., Zhanguo Wang, *Semiconductor diamond*, in *Ultra-Wide Bandgap Semiconductor Materials*, Elsevier, Editor 2019, Materials Today. p. 111-261.
19. Fontaine, F., et al., *Boron implantation in situ annealing procedure for optimal p-type properties of diamond.* Applied Physics Letters, 1996. **68**(16): p. 2264-2266.

.